Discrete dislocation plasticity analysis of single slip tension

Deshpande, VS; Needleman, A; Van der Giessen, E

Published in:
Materials science and engineering a-Structural materials properties microstructure and processing

DOI:
10.1016/j.msea.2005.02.087

Publication date:
2005

ELSEVIER

Materials Science and Engineering A 400–401 (2005) 154–157

MATERIALS SCIENCE & ENGINEERING A

www.elsevier.com/locate/msea

Discrete dislocation plasticity analysis of single slip tension

V.S. Deshpande[a,*], A. Needleman[b], E. Van der Giessen[c]

[a] *Cambridge University, Department of Engineering, Trumpington Street, Cambridge CB2 1PZ, UK*
[b] *Brown University, Division of Engineering, Providence, RI 02912, USA*
[c] *University of Groningen, Department of Applied Physics, Nyenborgh 4, 9747 AG Groningen, The Netherlands*

Received in revised form 23 November 2004; accepted 22 February 2005

Abstract

The effect of loading conditions on the tensile stress versus strain response of micron-sized planar crystals with a single active slip system is investigated via finite and small deformation discrete dislocation plasticity analyses. When rotation of the tensile axis is prevented, lattice curvature is induced in the crystal in both the small and finite strain analyses with the build-up of geometrically necessary dislocations resulting in a hardening response. The hardening rate is higher in the small strain analyses and this is attributed to the assumption of linear kinematics in that analysis. On the other hand, when rotation of the tensile axis is permitted, no lattice curvature is induced in the crystal in the small strain analysis resulting in an ideally plastic response. However, the change in the geometry of the crystal induces bending moments in the crystal in the finite strain analyses giving rise to a mildly hardening tensile stress versus strain response.

Keywords: Mechanical properties; Tension; Size effects; Computer simulation

1. Introduction

In recent years, considerable activity has been directed at experimentally investigating the behavior of micron-sized crystals with the aim of investigating plasticity size effects in the absence of macroscopically imposed strain gradients. For example, Hemker and co-workers [1,2] have pioneered a micro-sample testing methodology for investigating the room and high temperature tensile response of single and polycrystalline samples with widths $\geq 2\mu$m. More recently, Uchic et al. [3] investigated the compressive response of Ni single crystals oriented for single-slip deformation using a conventional nanoindentation device fitted with a flat-punch indentation tip. These studies report marked size effects with the tensile and compressive strength of the materials increasing with decreasing size.

The significance of boundary conditions on the tensile response of single crystals has long been recognized at least within the context of continuum plasticity: rotation of the crystal lattice changes the resolved shear stress on the slip systems and which, in turn, affects subsequent straining, see for example [4]. In this study, we employ finite and small strain discrete dislocation plasticity to investigate the effects of boundary conditions and lattice rotation on the tensile response of micron-sized single-slip system planar crystals.

2. Finite strain formulation

Deshpande et al. [5] presented a framework for analyzing finite deformation plasticity problems where plastic flow arises from the collective motion of discrete dislocations. The main assumptions in this framework are: (i) dislocation glide is the mechanism of plastic deformation, (ii) lattice strains remain small away from the dislocation cores and (iii) the elastic properties are unaffected by slip. The formulation accounts for: (i) finite deformation-induced lattice rotations and (ii) the effect of shape changes due to slip on the momentum balance. Thus, this formulation is ideally suited to investigate the effects of boundary conditions and lattice rotations on the tensile response of micron-sized specimens.

Similar to the small strain formulation in [6], the total displacement rate or stress fields are assumed to be given by a

* Corresponding author. Tel.: +44 1223 332664; fax: +44 1223 332662.
E-mail address: vsd@eng.cam.ac.uk (V.S. Deshpande).

0921-5093/$ – see front matter © 2005 Elsevier B.V. All rights reserved.
doi:10.1016/j.msea.2005.02.087

superposition of the analytically known fields of dislocations in an infinite medium and the complimentary fields that enforce the boundary conditions. In the finite strain analysis, the complimentary problem is nonlinear and is solved iteratively using an updated Lagrangian scheme. Readers are referred to [5] for further details.

3. Uniaxial tension with single slip

Plane strain finite and small strain discrete dislocation plasticity predictions for uniaxial tension with single slip are contrasted, for two sets of boundary conditions. We analyze an elastically isotropic crystal with Young's modulus $E = 70\,\text{GPa}$ and Poisson's ratio $\nu = 0.33$, which are representative values for aluminum. Consistent with the plane strain assumption, only edge dislocations are considered with Burgers vector $b = 0.25\,\text{nm}$, which does not change during deformation since the elastic stretch of the lattice is assumed to be negligible. The undeformed crystal is of dimension $2H \times 2W$, with $H = 2.0\,\mu\text{m}$ and $W = 0.5\,\mu\text{m}$, and has one slip system making an angle $\phi = 45^\circ$ with the positive x_1 axis. Initially, the crystal is free of mobile dislocations, but dislocations can generate from 60 sources that are equally dispersed over the slip planes. The sources nucleate a dipole when the Peach–Koehler force exceeds a critical value of $\tau_{\text{nuc}}b$ over a period $t_{\text{nuc}} = 10\,\text{ns}$; τ_{nuc} is taken to have a Gaussian distribution with a mean strength $\bar{\tau}_{\text{nuc}} = 50\,\text{MPa}$ and a standard deviation of 1 MPa. There is also a random distribution of 30 point obstacles with $\tau_{\text{obs}} = 150\,\text{MPa}$. The drag coefficient for glide is $B = 10^{-4}\,\text{Pa s}$, which is a representative value for several f.c.c. crystals and $L_e = 6b$. The finite deformation calculations are compared with results from small deformation calculations on identical crystals subject to the same boundary conditions, carried out as described in [7].

The tensile axis is aligned with the x_1 direction and tension is imposed by prescribing the displacement rates $\dot{u}_i$ and traction rates $\dot{T}_i$ as $\dot{u}_1 = \dot{U}$, $\dot{T}_2 = 0$ on $x_1 = 2H + U$, and $\dot{u}_1 = -\dot{U}$, $\dot{T}_2 = 0$ on $x_1 = -U$, where $U = \int \dot{U}\text{d}t$. The lateral edges, those initially on $x_2 = \pm W$, are traction free, i.e. $\dot{T}_1 = \dot{T}_2 = 0$. A time step of $\Delta t = 0.5\,\text{ns}$ is needed to resolve the dislocation dynamics so a rather high loading rate $\dot{U}/H = 2000\,\text{s}^{-1}$ is used. With these common set of boundary conditions we explore the effect of the constraint imposed by the tensile grips by considering in turn, the following two additional boundary conditions:

(i) Tensile axis rotation restricted: $\dot{u}_2 = 0$ is imposed on two material points at $(x_\epsilon, 0)$ and $(2H - x_\epsilon, 0)$ in the undeformed configuration, where $x_\epsilon = 0.1\,\mu\text{m}$. This simulates the constraint imposed by the grips which prevents the rotation of the line spanning $(x_\epsilon, 0)$ to $(2H - x_\epsilon, 0)$, referred to here as the tensile axis. This boundary condition is representative of those in the micro-sample tensile tests of Hemker and co-workers [1,2].

(ii) Tensile axis rotation permitted: $\dot{u}_2 = 0$ is imposed on one material point at $(2H - x_\epsilon, 0)$ in the undeformed configuration, where $x_\epsilon = 0.1\,\mu\text{m}$. This prevents rigid body translation in the x_2 direction but does not restrict the rotation of the tensile axis of the specimen. It is worth mentioning here that even though rotation of the tensile axis of the specimen is permitted, the applied displacements prevent the rotation of the ends of the specimen. This boundary condition is representative of those in the compression tests of Uchic et al. [3].

3.1. Tensile axis rotation restricted boundary condition

The nominal stress, σ_{nom}, versus strain, U/H, response of this single crystal employing the finite strain discrete dislocation plasticity framework is shown in Fig. 1a.

The first dislocation activity occurs at $\sigma_{\text{nom}} \approx 100\,\text{MPa}$ and is followed by a sharp decrease in the load followed by a fluctuating σ_{nom} versus U/H response up to $U/H \approx 0.01$. Subsequently, the specimen exhibits a linear hardening

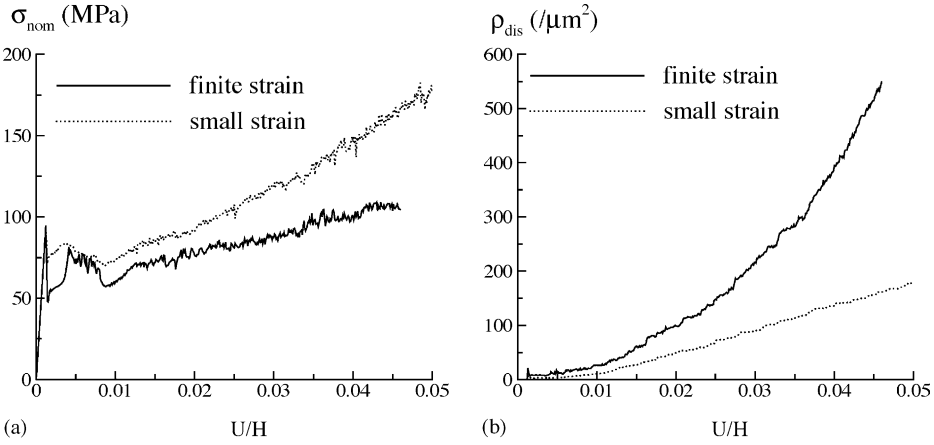

Fig. 1. Comparison between finite strain and small strain predictions for boundary condition with tensile axis rotation restricted. (a) Nominal tensile stress versus nominal tensile strain and (b) evolution of dislocation density with nominal strain.

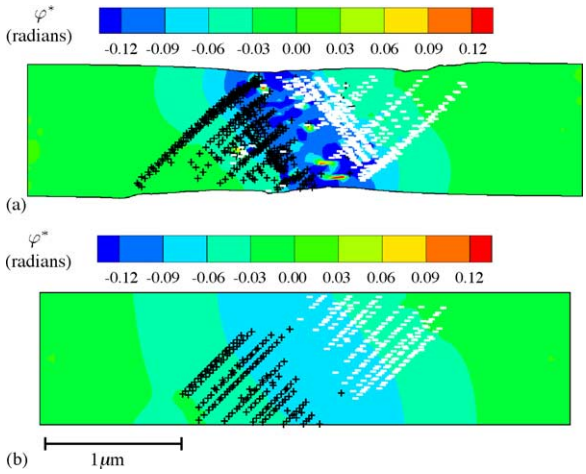

Fig. 2. Contours of the lattice rotation φ^* and the dislocation structure at $U/H = 0.045$ as predicted by the (a) finite strain and (b) small strain analyses for the boundary condition with tensile axis rotation restricted.

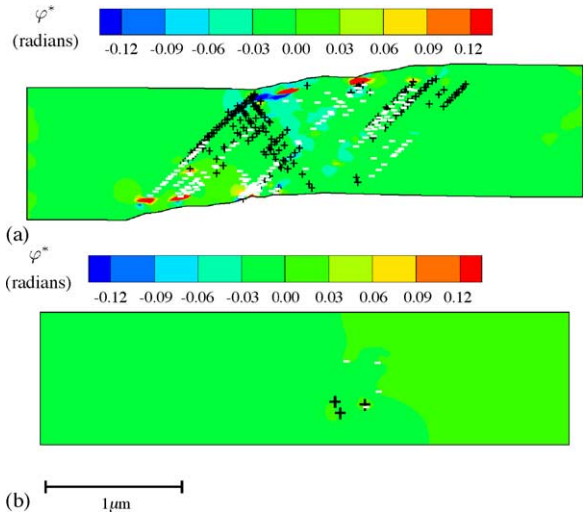

Fig. 4. Contours of the lattice rotation φ^* and the dislocation structure at $U/H = 0.05$ as predicted by (a) finite strain and (b) small strain analyses for the boundary condition with tensile axis rotation permitted.

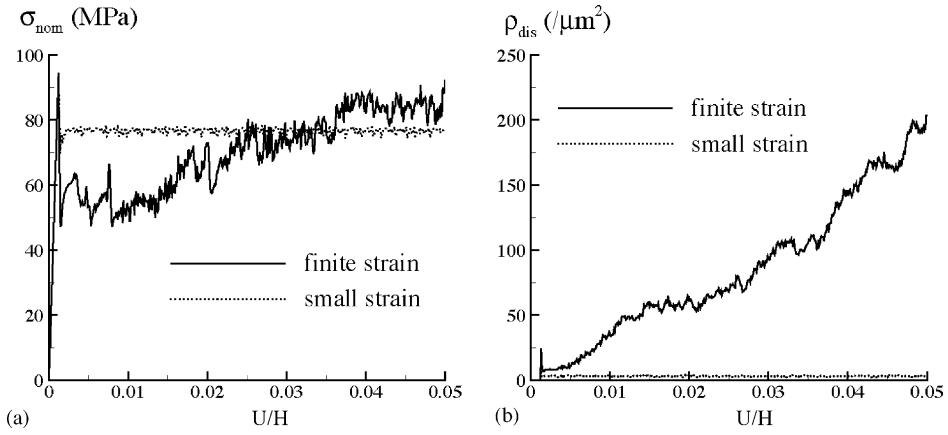

Fig. 3. Comparison between finite strain and small strain predictions for boundary condition with tensile axis rotation permitted. (a) Nominal tensile stress versus nominal tensile strain and (b) evolution of dislocation density with nominal strain.

response with a hardening rate $\mathrm{d}\sigma_{\mathrm{nom}}/\mathrm{d}(U/H) \approx G/30$, where G is the shear modulus of the crystal. The corresponding dislocation density ρ_{dis} (number of dislocations per unit area in a central 1 μm × 1.5 μm region) shown in Fig. 1b, increases approximately quadratically with U/H. For comparison purposes, the corresponding small strain discrete dislocation plasticity predictions are included in Fig. 1. The small strain analysis predicts a much higher hardening rate of the crystal, $\mathrm{d}\sigma_{\mathrm{nom}}/\mathrm{d}(U/H) \approx G/10$, and a lower dislocation density that increases approximately linearly with U/H.

The dislocation structures and contours of the lattice rotation φ^*, predicted by the finite and small strain analyses at $U/H = 0.045$ are plotted in Fig. 2a and b, respectively. In both cases, the constraint imposed by restraining the tensile axis to remain parallel to the x_1 axis results in the formation of a kink band at $\theta \approx -45^\circ$ with respect to the x_1 axis (i.e. perpendicular to the original slip direction). The finite strain calculation predicts an increased lattice rotation[1] within the kink band compared to the small strain analysis: since the density of geometrically necessary dislocations scales linearly with curvature, this is consistent with the higher dislocation density in the finite strain analysis. Further, curving of the slip system due to lattice rotations occurs only in the finite strain analysis. The large lattice rotations suggest the need to employ a finite strain formulation. The high hardening rate predicted by the small strain analysis likely arises from the assumption of linear kinematics.

3.2. Tensile axis rotation permitted boundary condition

The finite and small strain discrete dislocation plasticity predictions of the nominal stress versus nominal strain

[1] A positive φ^* corresponds to a counter-clockwise rotation.

response of the crystal, with boundary condition (ii) described above, are plotted in Fig. 3. Both the small and finite deformation analyses predict an initial peak stress of ≈95 MPa. Subsequently, the small strain analysis predicts an ideally plastic response with a flow strength ≈78 MPa. On the other hand, the finite strain analysis predicts a hardening response up to $U/H \approx 0.035$, beyond which σ_{nom} is seen to remain approximately constant at ≈84 MPa. The predictions of the evolution of ρ_{dis} with U/H are shown in Fig. 3b. While the finite strain analysis predicts that ρ_{dis} increases with U/H and rises to approximately $200\,\mu\text{m}^{-2}$ at $U/H = 0.05$, the small strain analysis predicts an almost constant dislocation density of about $4\,\mu\text{m}^{-2}$.

To rationalize these differences, the dislocation structures and contours of the lattice rotation φ^*, at $U/H = 0.05$ are plotted in Fig. 4a and b corresponding to the finite and small strain analyses, respectively. Large lattice rotations, $\varphi^* \approx -0.03$, are seen to develop in a band at $\theta \approx -45^\circ$ with respect to the x_1 axis in the finite strain calculations. The finite strain analysis accounts for the effect of geometrically changes on the momentum balance and thus the applied tensile stress induces bending moments in the specimen due to the deformations seen in Fig. 4a. These bending moments in turn induce the lattice curvature which results in the high dislocation density. Note that the lattice rotations with the tensile axis rotation permitted boundary condition are much smaller than those in Fig. 2a. In contrast to the finite strain predictions, no bending moments are induced in the small strain analysis as the framework does not include the effect of geometry changes on the momentum balance. Thus, the lattice rotations are seen to be negligible in the small strain analysis. The very low dislocation density predicted by the small strain analysis arises because the dislocations that are nucleated, exit this very small specimen very quickly with no dislocation storage due to the absence of induced strain gradients. On the other hand, shape changes induce bending moments in the finite strain analysis giving rise to lattice curvature, a build-up of dislocations, and a mildly hardening response.

Acknowledgements

Support from the Materials Research Science and Engineering Center at Brown University (NSF Grant DMR-0079964) and from EPSRC, UK (GR/S08107/01) is gratefully acknowledged.

References

[1] M. Legros, B.R. Elliott, M.N. Rittner, J.R. Weertman, K.J. Hemker, Phil. Mag. A 80 (2000) 1017.
[2] M. Zupan, M.J. Hayden, C.J. Boehlert, K.J. Hemker, Exp. Mech. 41 (2001) 242.
[3] M.D. Uchic, D.M. Dimiduk, J.N. Florando, W.D. Nix, Mater. Res. Soc. Symp. Proc. 753 (2003) BB1.4.1.
[4] R.J. Asaro, Adv. Appl. Mech. 23 (1983) 1.
[5] V.S. Deshpande, A. Needleman, E. Van der Giessen, J. Mech. Phys. Solids 51 (2003) 2057.
[6] E. Van der Giessen, A. Needleman, Modell. Simul. Mater. Sci. Eng. 3 (1995) 689.
[7] H.H.M. Cleveringa, E. Van der Giessen, A. Needleman, Int. J. Plast. 15 (1999) 837.